LRP 604/98 June 1998

PAPERS PRESENTED AT THE

SECOND EUROPHYSICS TOPICAL CONFERENCE ON RF HEATING AND CURRENT DRIVE OF FUSION DEVICES

BRUSSELS, BELGIUM, JANUARY 20 - 23, 1998

LIST OF CONTENTS

STATUS OF ELECTRON CYCLOTRON WAVE TECHNOLOGY

M.Q. Tran

Centre de Recherches en Physique des Plasmas
Association Euratom - Confédération Suisse
Ecole Polytechnique Fédérale de Lausanne
PPB-Ecublens, CH-1015 Lausanne, Switzerland

ABSTRACT

A review of the two-key technologies for the electron cyclotron wave (ECW) system, the gyrotron source and the window, is presented. In both fields, significant progress has been made to meet the requirements of heating and current drive systems planned for devices such as W7-X or ITER, namely 1 MW—CW in the frequency range 140 - 170 GHz. Gyrotrons in this performance range have been tested in long pulse (many seconds). With the use of diamond window, extremely long pulse (>>10 s) or true CW is possible. Tests presently under way confirm such promising behaviour of the window, paving the way towards the development of megawat CW tubes.

I) INTRODUCTION

The use of high power electron cyclotron wave (ECW) in fusion devices offers many advantages. Firstly, ECW can fulfill many functions. At the beginning of the discharge, it can provide breakdown and assist the plasma formation. Later during the discharge, the absorption of ECW gives localized heating and current drive as well as mode control. The physics is well understood: theoretical as well as numerical predictions are supported by many experimental results [see for example B. Lloyd, this Conference [1] and references therein]. The ECW may be launched from vacuum by remotely located antennas with no accessibility problem.

For ITER, ECW is considered for all of these functions. For breakdown and start-up assist, a multi-frequency system (between 90 and 140 GHz) at moderate launched power (less than 5 MW) in short pulse (a few seconds) is necessary. The multi-frequency need arises from the requirement that the ECW system should be compatible with the entire range of toroidal magnetic fields foreseen for the operation of ITER (4 - 5.6 T). For the heating and current drive functions, the ECW system should be able to deliver to the plasma 50 MW in CW regime at 170 GHz [2]. In the present design, gyrotrons of 1 MW—CW are considered as RF sources. The microwave beam from the gyrotrons is transmitted in evacuated, low-loss corrugated waveguides to the low-field side of the torus and is launched as an ordinary (O) mode. A barrier window prevents the diffusion of Tritium from the reactor. To be compatible with the operation of ITER at different magnetic fields, albeit the frequency of the source is constant, the launching antenna must have the capability of steering the RF beam in the toroidal direction (toroidal launching angle $\Theta \simeq 15 - 45^{o}$).

The technology of ECW has undergone continuous development throughout the recent years. High power (0.5 to 1 MW), high frequency (up to 170 GHz) sources operating in long pulse (many tens of seconds) or CW are or will be required for tokamaks and stellerators already built or under construction, and for ITER. As a result of these demanding specifications, not only tube technology but also RF windows both for the tube and for the torus have to be developed. Regarding the transmission system, in a reactor the

necessity to provide a confinement barrier in case of window leakage leads to the use of low-loss, closed transmission lines, whereas in present day experiment open quasi-optical transmission is acceptable. Similarly in ITER, the antenna, albeit remotely located from the burning plasma has to be carefully designed from the thermomechanical point of view to insure reliable operations. A discussion of some of these issues can be found in [2].

Among the required technological developments, the two critical ones concern the source and the window. The technology of evacuated transmission lines compatible with power level up to 1 MW has been developed and is used in many devices (DIII-D, TCV, Tore Supra) at 0.5 MW power level. For the components beyond the window (going from the source to the torus), the design of these in-vessel components and of the launcher naturally has to take into account the nuclear environment, although they will be well shielded from the direct view of the burning plasma and located relatively remote from it [2].

Presently the gyrotron is the reference source for an ECW system on present devices as well as on ITER. The free electron maser (FEM) is another possible high power millimeter wave source under consideration. This report will cover recent progress made in gyrotron (Section II). Recent FEM experiments and its implications for the development of an ECW system for a fusion reactor is discussed in the report by Verhoeven presented at this Conference [3]. Window approaches and the properties of the most promising materials will be covered in Section III. Section IV will discuss about other components in an ECW System.

II) THE GYROTRON

a) General Description

A gyrotron is an RF source which converts the rotational energy of relativistic electrons in a magnetic field $\underline{B}_0$ ($\underline{B}_0 = B_0\underline{e}_z$) into electromagnetic energy. It consists of an electron gun which produces a thin annular electron beam having a high kinetic energy component in the direction perpendicular to $\underline{B}_0$, a resonator where

the interaction between the wave and the electrons occurs, a converter which transforms the electromagnetic wave from the resonator into the output desired wave pattern and a collector where the spent beam is collected. In the following discussion, the main aspects of the gyrotron operation will be reviewed.

In a gyrotron the wave frequency ω is approximately equal to the relativistic cyclotron frequency Ω_R or its harmonic

$$\omega = \frac{n\, eB_0}{\gamma m_e} = n\Omega_R \quad n = 1, 2, 3 \qquad (1)$$

(γ is the relativistic factor. $\gamma \approx 1 + eV_b[keV]/511$, eV_b being the energy of the electron beam in keV). In engineering terms the frequency f in GHz is related to the magnetic field by the simple relation:

$$f\,[GHz] = 28\, n\, B_0[T] \qquad (2)$$

The physical mechanism responsible for the energy conversion is the electron cyclotron maser instability [3], which causes bunching of the electrons in the perpendicular momentum plane (p_x, p_y) due to the variation of the relativistic cyclotron frequency Ω_R as the electrons exchange their energy with the electromagnetic wave. The physical mechanism is simple to describe. In the absence of any bunching, before the interaction the components (p_x,p_y) of electrons are uniformly distributed on a circle of radius $p_\perp = \sqrt{p_x^2 + p_y^2}$. In the interaction with the electric field of the electromagnetic wave with frequency $\omega = n\Omega_c$ no net energy transfer will occur since as many electrons will gain energy from the wave than loose energy. Taking into account the relativistc cyclotron frequency, phase bunching can occur since electrons which gain (resp. loose) energy will have a lower (resp. higher) relativistic cyclotron frequency. An electron which lags (resp. leads) the wave phase is accelerated (resp. decelerated) in phase, leading to phase bunching. Simple integration of the relativistic equation of motion of electrons in the presence of $\underline{B}_c$ and of the electromagnetic wave shows that, in average, electrons will give (resp. loose) energy to the wave if the wave frequency is slightly smaller (resp. larger) than $n\Omega_{CR}$. The instability being convective, the energy transfer occurs in a resonant cavity which provides the feedback necessary for the instability to grow from the

noise. Since the frequency is mainly determined by the magnetic field B_o through Eq. (1), a certain freedom is left to the designer to select the mode of the resonant cavity. The two main criteria used in defining the mode (usually a cylindrical or a coaxial TE^{o}_{mn1} mode) are: 1) the ohmic heat flux density P_Ω which must be limited to a value less than about 20 to 30 MW/m^2; 2) the necessity to avoid the presence of neighbour modes which have too close resonant frequencies and, therefore, could be excited in competition with the desired mode. There exist also other technical constraints which need to be taken into account in the design of the tube such as the voltage depression in the electron beam in the cavity, the emitter current density, the maximum diameter of the cathode etc. The methodology to select the optimum mode, which is compatible with operation at a given frequency and at high efficiency η_{el} ($\eta_{el} \gtrsim 35\%$) is given in references [5-6]. The electronic efficiency η_{el} is defined as:

$$\eta_{el} = \frac{\text{Power of the electron beam converted in RF in the cavity}}{I_b V_b} \qquad (3)$$

$$\eta_{el} = \frac{\langle\gamma_{in}\rangle - \langle\gamma_{out}\rangle}{\langle\gamma_{in}\rangle - 1}$$

I_b and V_b are respectively the electron beam current and voltage where $< >$ denotes the average over all the electrons in the beam and the indexes in and out refer to input and output of the resonant cavity. η_{el} does not take into account the various losses in the gyrotron.

The mode choice is mainly dependent on the frequency: the higher the frequency, the higher the mode (i.e. the larger the value of the mode indexes m and n) in order to fulfill the condition regarding the ohmic loss $P_\Omega \lesssim 20 - 30$ MW/m^2 in the cavity walls. As a consequence, the density of competing modes increases and a scheme to increase the mode separation has to be devised. This leads to the introduction of the concept of the coaxial cylindrical cavity (referred hereafter as the coaxial cavity) which can provide mode suppression and hence better mode separation than a simple cylindrical cavity. Detailed calculations [7] show that at high frequency (e.g. 170 GHz) a coaxial gyrotron offers the potentiality of delivering higher power (up to 4 MW compared to 1.1 MW for a cylindrical cavity) while keeping the heat load on the cavity wall at the same value (Ohmic loss $\leq$ 1.5

kW/cm^2 with ideal copper) and achieving the same efficiency (around 35%). The same calculations repeated at 140 GHz predict a maximm power of 1.8 MW for a cylindrical cavity gyrotron and 6.4 MW for a coaxial cavity one [7]. All these calculations do not take into account the constraint on the window, which is the limiting factor for reaching high CW power. Higher power per tube for an ECW system requiring about 60 MW of installed power as the one of ITER offers clearly an advantage by reducing the number of ancillary equipments (superconducting magnets, modulation anode power supplies if required, control system) and, if this power is compatible with the window, by requiring a lower number of transmission lines. Therefore, while a cylindrical cavity gyrotron can be designed and built to meet the ITER specification of 1 MW per tube, the successful development of CW coaxial cavity gyrotrons would be a major step for the use of ECW in fusion reactors.

The use of an overmoded resonator also allows frequency tuning by adjusting the magnetic field B_0 on a time scale compatible with the superconducting magnet used to generate B_0, i.e. in the order of tens of seconds. Faster (in the order of ms) frequency tuning is possible by changing the beam voltage and hence the relativistic factor γ (cf. Eq. 1). Efficient energy extraction from the electron beam is achieved if the electron beam radius matches the radius of the maximum electric field of the electromagnetic mode of the cavity and if the electrodynamic properties of the resonator are adapted to the desired frequency. Many experiments have been performed using both cylindrical and coaxial resonators, which clearly indicate the frequency tunabillity of a gyrotron. The main issue in this respect is the availability of a broadband window.

The radiation from the gyrotron resonator is a rotating high-order mode TE_{mn}, corresponding to the cavity mode. Such a mode is not well suited for propagation either in free space nor in closed waveguide. In the latter case ohmic losses will be too high leading to unacceptable transmission loss. The recent development of converters allows the power to be converted into a gaussian beam compatible with propagation in corrugated waveguides, or other beam patterns compatible with the gyrotron window design e.g. rectangular beam profile to avoid excessive local power loss and hence thermal stresses [8]. Since the important quantity is the

power coupled into the transmission line, it is important to define the efficiency of conversion of the RF beams from the resonator mode to the gaussian mode with the right polarization (corresponding to the desired ordinary O, extraordinary X or the elliptically circularized mode required by the physics of the ECW-plasma interaction) and compatible with the coupling into the corrugated waveguide.

$$\eta_{conv} = \frac{\text{Power in the gaussian mode}}{\text{Power at the output of the cavity}} \quad (4)$$

neglecting all ohmic power loss.

The gyrotron efficiency is

$$\eta_{RF} = \eta_{elec} \times \eta_{conv} \times (1 - \Gamma_{ohmic}) \quad (5)$$

where Γ_{ohmic} is the fraction of ohmic losses in various components of the tube cavity, mode converter. Typcially η_{RF} is of the order of 30%.

The efficiency can be improved by implementing a depressed collector to recover part of the energy of the spent electron beam. The distribution function of the spent electron beam at the cavity output has an energy spread towards the low energy end of about 30 keV. Therfore a retarding potential $\Delta V \approx 30$ kV can be applied on the collector to "recover" part of the energy of the spent beam. With the use of a depressed collector, the electronic efficiency η^{Dep}_{Elec} is:

$$\eta^{Dep}_{RF} = \eta_{RF} \times \left[\frac{1}{1 - \frac{\Delta V}{V_b}}\right] \quad (6)$$

η^{Dep}_{RF} up to 50% or higher has been achieved in existing gyrotrons. Higher efficiency could be achieved by using a multi-stage depressed collector, but at the expense of a more complex design.

An increase of the total gyrotron efficiency is crucial for a reactor or for any large ECW system, since it reduces the required electric circulating power. More over the use of a depressed collector also alleviates the total heat load on the collector and the requirements on its cooling, from about 2 MW (η_{RF} = 30%) to 1 MW (η^{Dep}_{RF} = 50%)

in the case of a 1 MW gyrotron. The requirement on the stabilty of the high power, high voltage power supply is also reduced, since the beam voltage can be supplied by a well-regulated low power high voltage supply which must only provide the body current.

b) Recent Development

At this point of the review, it is appropriate to summarize the performances achieved recently with gyrotrons. Table I gives the results obtained by long pulse tubes under development. For a review of the state of the art the interested reader can refer to Refs. [9-13]. It is important to point out that high power (0.5 - 1 MW) has been achieved at high frequency ($f \gtrsim 1$) of (110 - 170 GHz) at short or moderate pulse (up to seconds). In some cases the pulse length extension is limited by the window. When the window is compatible with long pulse or CW operation, such as in the case of the 118 GHz gyrotron with a liquid Nitrogen-cooled sapphire window or the Toshiba - JAERI tube with a water-cooled diamond window, work is in progress to lengthen the pulse. It is worth noting that long pulses or CW operation of a gyrotron has required a careful thermal and thermomechanical design, taking into account possible electro-magnetic radiation leakage and/or components subject to heat load and having very long thermal time constant ($\gtrsim$ 60 s). As mentioned before, different window schemes are already implemented in long pulse tubes and that they range from cryogenically-cooled sapphire (at liquid nitrogen temperature) to diamond-cooled by water flowing at its edge. This subject will be discussed in more detail in the following section.

The frequency tunability of gyrotrons has been shown in many experiments using gyrotrons with both cylindrical and coaxial cavities. As an illustration, Figure 1 shows the output power as the magnetic field B_0 is swept. The variation in power is mainly caused by the resonant character of the window: with a Brewster window, the output power remains constant as the magnetic field is changed.

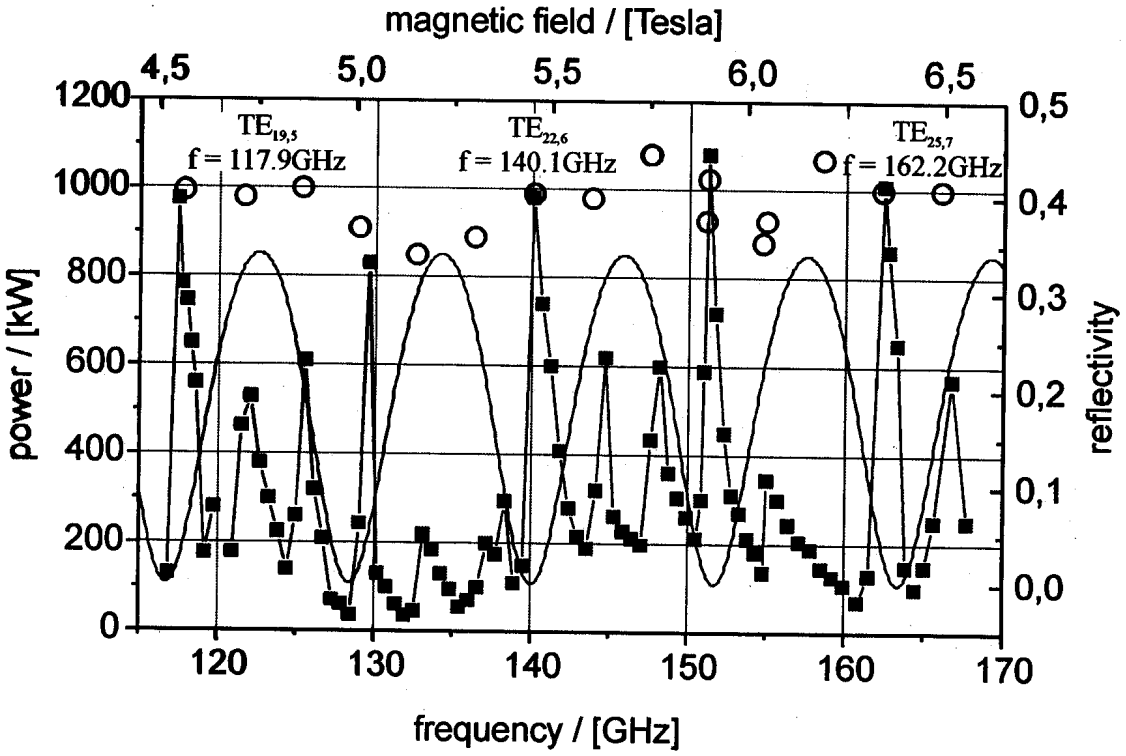

Figure 1

Frequency tunability of a gyrotron. The squares correspond to the output measured with a conventional resonant window (6.58 mm thick; fused quartz). The open circles to those obtained with a broad-band Brewster window (7mm thick; fused quartz). The experiment was performed at the Forschungzentrum Karlsruhe.

Efficiency enhancement with a depressed collector has also been shown. The first experiments were performed by biasing the collector through a resistor to ground. More recently, experiments were performed in a realistic configuration, i.e. one where the main high voltage, high current power supply delivered only a fraction of the beam voltage [10]. The accelerating voltage was supplied by a high voltage low current supply. An efficiency of 48% was achieved. Experimentally it was shown that the regulation of the main high power supply (i.e. the one delivering the electron beam current) could be strongly relaxed: whereas in a gyrotron without a depressed collector, the cathode voltage regulation must be around ±0.5%, a voltage fluctuation up to 15% was allowed for the main high voltage power supply without negative effect on the stability of the gyrotron operation.

Institution	Frequency [GHz] (Cavity mode)	Power [MW]	Efficiency [%]	Pulse length [s]
CPI	110 ($TE_{22,6}$)	1.09	32	0.6
		0.53	30	2
GYCOM	110 ($TE_{15,4}$ and $TE_{19,5}$)	0.5	33	0.5
		0.8		2
	170	0.95	31	0.1
	170	0.77	33	1 *
	170 ($TE_{25,12}$)	0.6	30	2 *
TTE, CEA, CRPP FZK	118 ($TE_{22,6}$)	0.53	32	5+
TOSHIBA, JAERI	170	0.5	36**	0.05*
	170	0.5		1.9 ++

Table I

Performances of long pulse gyrotron achieved at the time of the Conference (January 1998). It is important to note that progress in the test of the long pulse gyrotron is extremely rapid and many results will be obsolete by the time of publication of this paper.

* : *Limited by the window capability;*

** : *Efficiency with depressed collector;*

\+ : *Sapphire window at 80° K, the pulse enlargement is underway;*

++ : *Diamond window, the pulse enlargement underway.*

In parallel with the developement of the cylindrical cavity gyrotron, research in the field of coaxial cavity gyrotron confirms the potentialities of this concept as a high power microwave source. Experiments were performed in short pulse (from a few μs to a few ms) in the frequency range 100 GHz to 167 GHz. The cavity mode is $TE_{m,n}$ with m in the range of 20 to 32 and n around 13 to 18 [see for example Ref. 7]. Power in excess of 1.5 MW was obtained at 140 GHz at an efficiency of 33% with a $TE_{28,16}$ coaxial cavity and an output in

the same mode [9, 13]. At a frequency, 165 GHz, close to the one required for ITER, 170 GHz, 1.17 MW at an efficiency of 27% was obtained using a coaxial gyrotron operating in the $TE_{31,17}$.

III) WINDOW DEVELOPMENT

For fusion application, the availability of a suitable window for both the gyrotron and the torus is a crucial issue. A window is necessary to insure the integrity of the tube during its manufacture, its handling and storage. A window-less operation of the transmission line while implemented on a few existing devices (e.g. DIII-D, TCV and Tore Supra) cannot be considered for a reactor such as ITER since Tritium confinement has to be provided.

A suitable window material must have a low dielectric loss factor $tg\delta$ at the operating frequency, good thermal conductivity and mechanical properties. In the case of the torus window the above properties should be maintained under the neutron irradiation escaping from the reactor, although in the case of an ECW system one has the freedom to locate the window remotely from the plasma thus strongly lowering the neutron fluence and the energy spectrum of the neutrons. In the present design for ITER, the neutron fluence at the location of the window is around 10^{20} neutron per square meter. Tritium permeation is another important property since the window must act as a containment barrier. Last, but not least, brazing technology compatible with the high temperature ($\geq 500^{o}C$) of the baking cycle of the gyrotron must be developed to insure the proper manufacturing of the window assembly and its implementation on the tube.

For high power (>0.5 MW), high frequency application only a few materials are adequate. The use of sapphire requires either low temperature (a liquid nitrogen edge cooled window was implemented on the 118 GHz, 0.5 MW gyrotron, which was tested up to 5 s pulse length; extension to 1 MW power level at higher frequency necessitates that the window be cooled to liquid neon temperature) or advanced window geometry (distributed window concept or curved window [14]). A review of the status of window development can be found in Ref. [15]. In recent years, diamond has

received considerable attention due to its outstanding properties: low loss tgδ, high heat conductivity and its good mechanical properties. Large, "clear" (as opposed to the easier to produced "gray") diamond disk can now be commercially produced using CVD process. Measurement of tgδ performed at 140 GHz on large diamond disk (Diameter = 100 mm, thickness ≤ 2.5 mm) commercially produced by industry gives a value of tgδ as low as 10^{-5} uniform across the disk diameter. During test, this value remains unaffected by neutron irradiation up to 3.10^{20} n/m^2 nor γ or X rays up to 0.8 Gy/s. The heat conductivity coeffiecient is as high as 2100 W/m.K, or about 5 times that of copper. Calculations made at the Forschungzentrum Karlsruhe using these data show that 2 MW in gaussian mode could be transmitted through a 80 mm window inserted in a corrugated waveguide (I.D. = 52 mm, O.D. = 62 mm): the maximum temperature is about 340° K in the center using room temperature water cooling at the edge (coefficient of heat exchange = 12000 $W.m^{-2}.K^{-1}$). No significant change of the maximum temperature is achieved if the window diameter is enlarged to 100 mm while keeping the waveguide diameter constant. This calculation bears a very important consequence on the cost of the window since the price of the diamond disk increases rapidly with the diameter. Using a newly-developed technology for brazing diamond to metal, a diamond window was built and incorporated in a gyrotron developed by Toshiba and JAERI. At the time of this Conference, tests at 0.5 MW up to 1.9 s have been successfully performed and the extension of pulse length to many seconds is under way. Using a focused beam, tests at lower power (300 kW, 110 GHz, 1 s) corresponding to the power density of 0.8 MW in a HE_{11} mode have also been performed by the US company CPI and the Dutch research institute FOM. Similar tests have been performed by General Atomic (USA) and Gycom (Russian Federation) confirming the expected behaviour of a diamond window. Tube manufacturers are now implementing diamond windows in their tubes.

Doped Silicon is another material which has a low tgδ (tgδ < $3\ 10^{-6}$ at 200° K, i.e. at a temperature somewhat below the room temperature which could be easily achieved). Brazing technology has equally been developed for silicon and window assembly and has been built to test this concept at high power.

IV) TRANSMISSION LINE AND ANTENNA

Transmission line technology is well developed and is widely tested on present-day experiments. The RF waves can be transported either in closed waveguides or via mirrors (quasi-optical propagation). For ITER the necessity to provide a Tritium barrier leads to the choice of an evacuated waveguide. An evacuated waveguide has been used in DIII-D, TCV and is being implemented in Tore Supra. In these cases, its use allows to avoid the implementation of a vacuum window on the torus side, which could increase the complexity since either the beam profile at the window is not gaussian (TCV) or the window requires cryogenic cooling (TCV and Tore Supra). Quasi-optical propagation is implemented for example in the ECW of RTP and is planned for the stellarator W7-X. In a typical layout of a closed waveguide transmission line, such as the one of TCV [16], the polarization (elliptical polarization) and the pattern (size and location of the beam waist) of the RF beam are first controlled via respectively corrugated mirrors and focusing ones. The line itself consists of HE_{11} corrugated waveguides, miter bends with or without power monitor, bellows, DC break, pumping tees, RF switches and loads. The thermal expansion of the plasma vacuum vessel as well as the unavoidable mismatch in the length of the corrugated waveguide are taken care of by the bellows. In the case of TCV, the transmission line with a diameter of 63.5 mm (2.5 inches) was designed to transmit more than 0.5 MW. Operation at the nominal power of 0.5 MW in pulse of more than 1 s was achieved with the tokamak operation without any special conditioning (either RF or baking) of the line. On DIII-D, long pulses at 1 MW of power have been routinely handled in an evacuated waveguide of diameter 31.7 mm, for an average power density of 125 kW/cm^2.

For ITER where beam steering is necessary since the machine will be operated at different toroidal magnetic fields, the launcher must be carefully designed since it combines cooling circuit and moving parts which are in the neighbourhood of a reacting D-T plasma. Preliminary studies of such a launcher are being performed by ITER partners and solutions have been proposed, which take into account the various operational constraints imposed by ITER.

Another important issue to be considered is the operation, the

availability and the reliability of a large ECW system at high power. For a device like ITER, the number of gyrotrons and transmission lines will be of the order of 60 to 70 and the total power delivered to the plasma is 50 MW for the heating and current drive function. Systems delivering between 4.5 and 10 MW using up to 10 tubes and transmission lines are being implemented or are planned. Undoubtedly they will bring interesting information about the operation of large ECW systems and provide important information about the availability and reliability of ECW systems.

V) CONCLUSION

Recent advances in the technology of the ECW system in the two critical fields of the RF source and window show the feasibility of a multi-megawatt ECW system for fusion experimental devices. A MW gyrotron in the frequency range of interest for ITER is now under development and test. Some gyrotrons already incorporate diamond windows which can transmit at least 1 MW—CW. Technology of transmission lines is far advanced so no major difficulties are expected to be encountered in this field.

Acknowledgement

The author would like to thank Drs. G. Denisov, T. Imai , A. Litvak, M. Makowski, R. Prater, R. Temkin, M. Thumm, A.G.A. Verhoeven for their contribution to the presentation at the Conference and to this report. The hospitality of the Institut für Plasma Physik of the Forschungzentrum Jülich, where part of this report was prepared, is also greatly acknowledged.

This work was partially supported by the Swiss National Science Foundation.

REFERENCES

[1] Lloyd B., 1998, Proceedings of Invited Paper of this Conference.

[2] Makowski M., 1996, IEEE Trans. PS24, 1023.

[3] Verhoeven A.G.A., 1998, Proceedings of Invited Paper of this Conference.

[4] Chu K., Hirshfield J. L., 1978, Phys. Fluids 21, 461.

[5] Tran M.Q., Tran T.M., Whaley D.R., Iatrou C., Kern S., Möbius A., Nickel H.U., Norajitra P., Thumm M., Bon Mardion G., Pain M., Tonon G., 1994, Conf. Digest 19th International Conference on Infrared and Millimeter Waves, Sendai, Japan, p. 67.

[6] Iatrou C., Whaley D.R., Kern S., Thumm M., Tran M.Q., Möbius A., Nickel H.U., Norajitra P., Wien A., Tran T.M., Bon Mardion G., Pain M., Tonon G., 1995, Int. J. IR & MM Waves 16,1129.

[7] Kern S., Iatrou C.T., Proceedings of the 21st International Conference on Infrared and Millimeter Waves, Berlin 1996, Editors: von Ortenberg M. and Mueller H.U., ISBN 3 00 00800-4, Paper ATh12.

[8] Bogdanov A.A., Chirkov A.V., Denisov G.G., Vinogradov D.V., Kuftin A.N., Malygin V.I., Zapevalov V.E., 1995, Int. J. IR & MM Waves 16, 773.

[9] Thumm M., State of the Art of High Power gyro devices and Free Electron Masers, Update 1997, Wissenschaftliche Berichte FZKA 6060, Forschungzentrum Karlsruhe GmbH, Karlsruhe 1998.

[10] Tsuneoka M., Fujita H., Sakamoto K., Kasugai A., Imai T., Nagashima T., Asaka T., Kamioka N., Yasuda M., Iiyama T., Yoshisa T., Nara H., Ishibashi M., 1997, Fusion Eng. Design 36, 461.

[11] Prater R., Austin M.E., Bernabei S., Callis R.W., de Grassie J.S., Lin-liu Y.R., Lohr J.M., Luce T.C., Murakami M., Petty C.C., Pinsker R.I., Ponce D., Zerbini M., 1998, Proceedings of the 2nd Europhysics Topical Conferences on Radio Frequency Heating and Current Drive of Fusion Devices, 1998, Europhysics Conference Abstracts Vol. 22A, Editors: J. Jacquinot, G. van Oost, R.R. Weynants, p. 221.

[12] Thumm M., 1997, Radio Frequency Power in Plasmas, 12th Topical Conference, Savannah, 1997, AIP Conference Proceedings 403 (AIP, 1997), p. 183.

[13] Flyagin V.A., Khizhnyak V.I., Kuftin A.N., Manuilov V.N., Pavelyev A.B., Pavelyev V.G., Zapevalov V.E., Conf. Digest 22nd International Conference on Infrared and Millimeter Waves, Wintergreen, Virginia, USA, 1997, p. 112.

[14] Hadelmann G.S., Conf, Digest 22nd International Conference on Infrared and Millimeter Waves, Wintergreen, Virginia, USA, 1997, p. 152.

[15] Thumm M., Conf. Digest 22nd International Conference on Infrared and Millimeter Waves, Wintergreen, Virginia, USA, 1997, T 4.1.

[16] Goodman T.P., Henderson M., Perthuisot F., Pietrzyk Z.A., Pochelon A., Tran M.Q., Hogge J.Ph., Moret J.M., Sauter O., van Toledo W., Razumova K.A., Proceedings of the 2nd Europhysics Topical Conferences on Radio Frequency Heating and Current Drive of Fusion Devices, 1998, Europhysics Conference Abstracts Vol. 22A, Editors: J. Jacquinot, G. van Oost, R. R. Weynants, p. 245.

Influence of Polarization in ECCD Experiments in TCV

T.P.Goodman, M.A.Henderson, F.Perthuisot, Z.A.Pietrzyk, A.Pochelon, M.Q.Tran, J-Ph.Hogge, J-M.Moret, O.Sauter, W.van Toledo, K.A.Razumova†

Centre de Recherches en Physiquedes Plasmas, Ecole Polytechnique Fédérale de Lausanne Association EURATOM-Confédération Suisse, CH-1015 Lausanne, Switzerland

† Russian Research Center Kurchatov, 12182 Moscow, RF

Introduction - First and second harmonic electron cyclotron current drive (ECCD) has been studied worldwide for many years: it has proven difficult to measure the true EC current drive. There is often a residual electric field present during the experiments leading to current associated with the "induced" conductivity. In addition, a significant portion of the current can be carried by the bootstrap current I_{BS} since the ECCD tends to create steep gradients due to the high degree of localization of the power. Ignoring these additional sources of current leads to over-estimates in the measurements of EC current drive. Alternately, because the EC current I_{EC} is carried largely by the high energy tail of the electron distribution, there may be a significant reduction in the measured currents if the slowing down time of these high energy electrons is longer than their confinement times [Alikaev 95]. When experiments are carried out with full current replacement (no residual electric field), a so-called non-inductive current drive can be determined which is the sum of the EC current drive and the I_{BS}. If sufficient measurements are available, the I_{BS} contribution can be calculated and the "pure" EC current can be determined [Petty 95].

Experiments to date have used fixed polarization of the launched EC power (often linearly polarized as a first approximation to pure X-mode coupling) and have then concentrated on the comparison of the results to linear theory and Fokker-Planck (FP) codes such as CQL3D or OGRAY. The TORAY (linear with relativistic and trapped particle effects) ray tracing code is often used as a baseline for comparison. Only recently, on DIII-D, have measurements of 2nd harmonic current drive been shown to agree with non-linear theoretical calculations: previous experiments reported lower currents than expected [Petty 95].

Experimental Setup - Initial ECCD experiments on TCV have concentrated on the influence of *elliptical polarization* on plasma performance and current drive efficiency. These experiments provide a check of the system performance as well as a reference experiment with small, close-to-circular, moderate-q_a plasmas (κ=1.17, δ=0.07, q_a=4.6, I_p=158kA, $n_{eo}=2.0\times10^{19}m^{-3}$), before investigating shaped plasmas. Current and density are feedback-controlled and changes in surface loop voltage provide the main diagnostic for evidence of current drive (with all of the above mentioned problems associated with the interpretation of the measurements).

Power was provided by one gyrotron at the second harmonic (0.5 MW, 82.7 GHz, 0.6s, X2) of the cyclotron resonance. The transmission system includes a 2-mirror low-incidence angle universal-polarizer immediately after the gyrotron and a multihole power

monitor approximately 2/3 of the way to the tokamak. The power monitor (PM) is cross calibrated with a calorimetric load placed as close to the tokamak as possible (~3m from launcher). The polarizer is mechanically zeroed for linear polarization and a polarizer mirror angle scan is done to verify the zeros angles of both mirrors (zero power measured within cross-talk of the receivers at the PM confirms the zero of one mirror and the peak power indicates the other). The calorimetric power remains constant during the scan indicating no losses associated with polarization rotation. The PM measurements provide a validation of the polarization change during the ECCD experiments but do not provide confirmation of the correctness of the calculated coupling to the X-mode [Smits 93]. This is confirmed by the plasma response, as shown in the following section.

The TCV vacuum vessel can accommodate plasmas with elongations of up to κ=3 but in these experiments, the plasma was placed in the upper half of the vessel directly in front of the antenna to allow low-field-side launch in the plasma midplane. The antenna [Goodman 96] is highly versatile allowing changes between ECRH, CO, or COUNTER - ECCD from shot to shot. It should be noted that, unlike other experiments (e.g. T-10 and DIII-D), the plasma current is not reversed when changing from CO to COUNTER ECCD.

TORAY calculations indicate that a maximum in current drive efficiency occurs near 20° from the radial; therefore, this was the injection angle used during the experiments. Absorption occurs at the magnetic axis for this angle and the moderate densities used in these experiments. The beam is modeled by 30 rays with a free-space beam divergence and spot size that match those of the experimental beam at the plasma center. The X-mode is fully absorbed on the LFS of the resonance and shows slight refraction. The O-mode is poorly absorbed (<12%) and refraction is negligible over the short path lengths required to traverse the plasma and strike the inner wall. The incomplete power absorption leads to a current drive efficiency for the O-mode portion that is ~4 times smaller than the average absorption might suggest – in the same direction as the X-mode current drive. Maximum current drive efficiencies of $\eta \equiv I_p/P_{abs}$ of 5.8×10^{-2}[A/W] (co) and 7.8×10^{-2}[A/W] (counter) are calculated for the experimental values of plasma current I_p and maximum absorbed power P_{abs} (assumed to be equal to the launched power of 0.5MW). The difference is as expected from linear theory $\eta \propto T_e/\left(n_e R_o (Z_{eff}+5)\right)$ given the differences in electron density and temperature (major radius R_o and effective charge Z_{eff} remaining constant) for the shots.

Evidence of ECCD - All signals (T_e , n_e , V_{loop}, etc.) were averaged over the last 0.2s of the 0.6s EC pulse during ECRH and CO and COUNTER ECCD to reduce the noise in the measurements. The results are plotted as a function of the X-mode power fraction f_x defined as the power coupled to the X-mode divided by the (constant) input power of 0.5MW. The coupling is calculated, as mentioned above, in the zero density limit using the experimental

magnetic field angles at the edge calculated from LIUQE reconstruction code data. It is assumed that the X- and O-mode power travels independently after entry in the plasma.

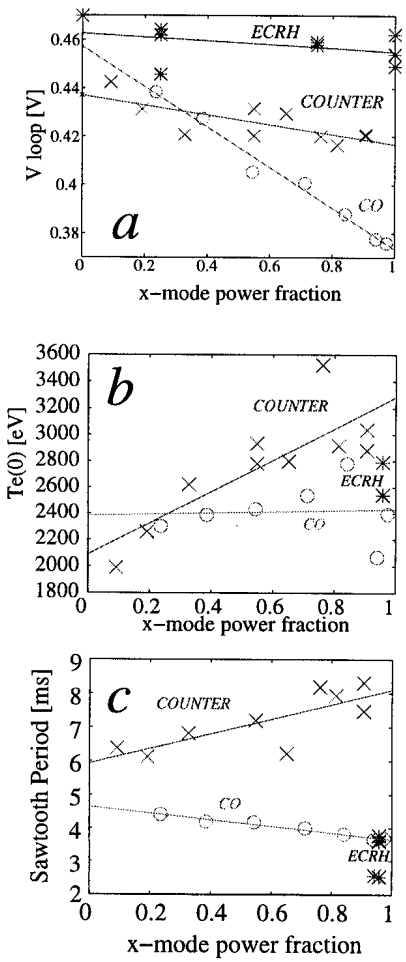

Figure 1 Response of a) loop voltage, b) central electron temperature and c) sawtooth period during polarization scan.

In figure 1a, loop voltage is seen to *decrease* with *increasing* X-mode fraction for *both* co and counter launch. This is to be expected for co current drive as more current is being driven: intuitively, counter current drive should produce the opposite effect. V_{loop} does not change significantly with polarization for ECRH indicating that only heating occurs. Central electron temperature (Fig. 1b) is found to be roughly independent of polarization for co-ECCD and ECRH (indicating that transmitted O-mode power is eventually absorbed by the plasma rather than lost); however, as coupling to the X-mode is increased during counter-ECCD, the central electron temperature rises dramatically. (During these scans the formation of a hot ion tail is seen by the neutral particle analyzer and is strongly polarization dependent - showing an increase similar to electron temperature for counter but, also, to a lesser extent for co-ECCD.) Since current drive efficiency increases with temperature, the decrease in V_{loop} with X-mode power fraction is even more surprising. On the other hand, plasma conductivity is increasing $\sim T_e^{1.5}$ so that the net effect could be a decrease in V_{loop}. I_{BS} is most likely acting opposite to the counter current drive and if large enough could also lead to the observed behavior in V_{loop}. In spite of the uncertainty about the behavior of the driven current, clear evidence of *current profile modification* is seen on the X-ray traces. In particular the sawtooth period *increases* (Fig. 1c), amplitude *decreases* (Fig. 2) and inversion radius *decreases* (relative to the ohmic phase) with increasing X-mode fraction. The first two features have been associated with sawtooth stabilization due to increasing counter current during a density scan on T-10 [Alikaev 95]. The third feature by itself may not indicate counter current drive; however, the inversion radius for high X-mode fraction ECRH and co-ECCD *increases* rather than decreases. It should be noted that the heating location is just inside the inversion radius at highest X-mode fraction and that sawtooth stabilization has been observed during ECRH when heating on the inversion radius [Pietrzyk 98].

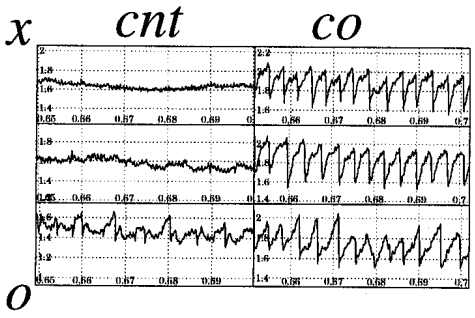

Figure 2 Sawtooth shape for counter (left) and co (right) ECCD as X-mode power fraction is increased (bottom to top). For counter ECCD, sawteeth are stabilized while for co-ECCD the shape changes very slightly.

The co-ECCD plasma is much less sensitive to the changes in X-mode fraction and is quite similar to an ECRH plasma. The sawtooth period decreases (to the ECRH value at "pure" X-mode launch) (Fig. 1c) while the amplitude remains constant (Fig. 2) with increasing X-mode fraction. This along with the constant central temperature allows us to conclude that mode conversion and reflection from the inner wall of the chamber results in very little current drive since at low X-mode fraction, it should produce counter-like sawteeth. (Note that the shape of the sawteeth is very different during counter injection even at low X-mode fraction - lower left in figure 2). Therefore, the linear dependence of V_{loop} on X-mode fraction can be considered a feature of the current drive efficiency $I_{EC} = \eta \bullet P_{launched} \bullet f_x$. If one assumes a constant resistivity (neoclassical and induced) and I_{BS} during the co-ECCD scan, the current drive efficiency can be calculated from linear fit parameters: $V_{loop} = \left(I_p - I_{BS}\right)/R - \eta P_{launched}/R \bullet f_x$. The result is $\eta = 5.8\times10^{-2}[A/W]$. Note that although this value is the same as the TORAY value, TORAY does not include the effects of I_{BS}. The current drive efficiency will be reduced by a factor $(1-I_{BS}/I_p)$. At present, the available measurements do not allow an accurate calculation of the bootstrap fraction but allow an estimate of 10-20% to be made. Quasi-linear FP calculations are not yet available for comparison.

Conclusions - Power monitor measurements coupled with clear evidence (in the sense expected) of co-ECCD have confirmed the proper operation of the ECCD system and the strong influence of polarization on ECCD. Secondary evidence by sawtooth period, amplitude and inversion radius changes has strongly suggested the existence of counter-ECCD. The loop voltage measurements may be masked by large changes in temperature. A current drive efficiency of $5.8\times10^{-2}[A/W]$ has been measured and scales linearly with first pass absorbed power. This value is close to the value calculated from linear theory.

This work was partially supported by the Fonds National Suisse pour la Recherche Scientifique.

References

Alikaev, V.V., et al., Nuclear Fusion, Vol. 35, No. 4, 369, (1995)

Goodman, T.P., et al., 19th SOFT, Lisbon, 565, (1996)

Petty, C.C., Nuclear Fusion, Vol. 35, No. 7, 773, (1995)

Pietrzyk, Z.A., et al. (this conference)

Smits, F.M.A., (EC-8) Proc. 8th Joint Workshop on ECE and ECRH, Gut Ising, 549, (1993)

Central Relaxation Phenomena during Electron Cyclotron Heating in TCV

Z.A. Pietrzyk, A. Pochelon, T.P. Goodman, M. Henderson, H. Reimerdes, M.Q. Tran, R. Behn, I. Furno, J-P. Hogge, J. Rommers, O. Sauter, W. van Toledo, K.A. Razumova†

Centre de Recherches en Physique des Plasmas, Ecole Polytechnique Fédérale de Lausanne
Association EURATOM-Confédération Suisse, CH-1015 Lausanne, Switzerland

† Russian Research Center Kurchatov, 12182 Moscow, RF

A tokamak plasma is MHD unstable near its center in the region where q<1 leading to the well known sawtooth oscillations. This instability plays a beneficial role by removing impurities from plasma. However, it may also be detrimental as it reduces the energy content of the plasma. In case of «monster sawteeth » it can limit the plasma performance and be dangerous for vessel walls; therefore, control of these instabilities is desirable. This would imply control of the sawtooth period and/or shape of the sawteeth, since some shapes may be more beneficial for plasma performance. ECRH and ECCD are useful tools for such control.

This paper describes some preliminary observations of changes in sawtooth shape and period due to ECRH in TCV. To investigate the effect of heating location on sawtooth shape and period, the resonance position was varied by changing toroidal magnetic field or plasma vertical position (more than 25 cm) in the vessel

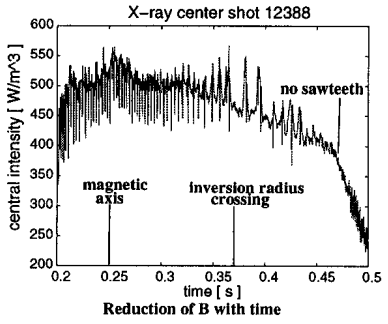

a)

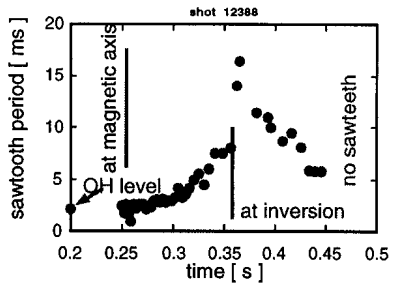

b)

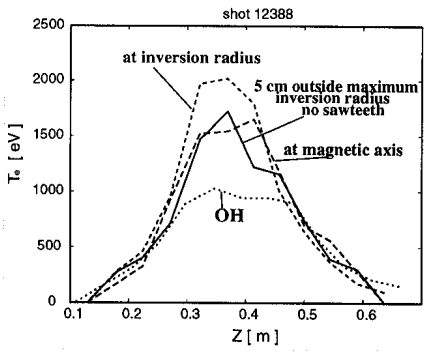

c)

Figure 1 Variation of heating location from magnetic axis to 10 cm outside of inversion radius by sweeping B field. a) X-ray central emissiviy, b) sawtooth period, c) temperature profiles for heating location near the center, inversion surface and at sawtooth disappearance.

during a shot , or the launch angle of the microwave beam on a stationary plasma. Results of all 3 types of sweeps are similar. As shown in Figure 1, sawtooth shape and period depend on localization of the heating with respect to the inversion radius (associated with q=1). Heating near the magnetic axis produces saturated sawteeth (in which central X-ray radiation increases rapidly after a crash, then suddenly saturates and stays almost constant until the next crash), which with increasing distance from the center, change to 1) normal (triangular) sawteeth, 2) humpbacks near the inversion surface, again 3) normal sawteeth and eventually to 4) full stabilization (no crashes). By sweeping the plasma heating location (0.3 cm/ms to 1.5 cm/ms) in both directions, no hysteresis was observed with respect to temperature, sawtooth shape, sawtooth period, or inversion radius.

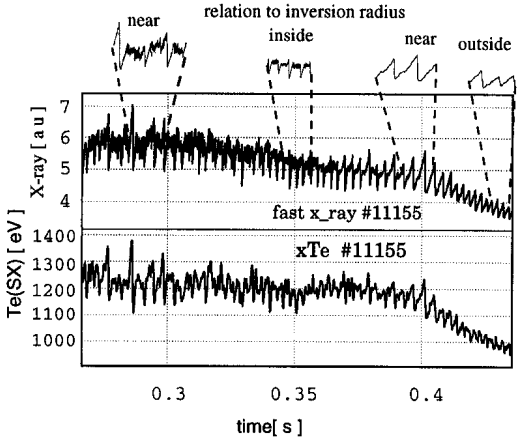

Figure 2 Change of soft X-ray flux and X-ray temperature as a function of time in during vertical displacement (by 28 cm) of the plasma. The heating location moved from the lower part to the upper part o of the inversion surface.

The sawtooth period and inversion radius remain constant when heating on the lower or the upper part of the inversion surface, (see Fig. 2.); however, the sawtooth shape changes from saturated to normal (triangular), respectively.

Full sawteeth stabilization can be obtained either by an increase of the sawtooth period to period longer than the heating pulse (this is possible with q(0)<1), or by reducing the sawtooth period to zero. Preliminary indications are that the first type of stabilization (creating a stable plasma by changing the current profile with q(0)<1), is obtained by heating near q=1 the second, with heating outside q=1.

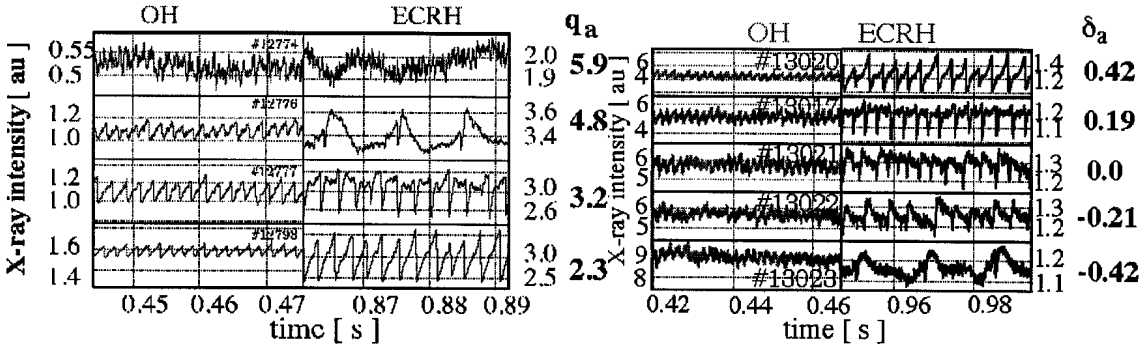

Figure 3. Change of sawteeth shape during q_a and δ_a scans.

The change of sawtooth shape and period, also depends on the values of q_a and δ_a, as shown in figure 3, as well as the density and heating power. The magnetic field was held constant in both q_a and δ_a scans, causing a change of the distance between the heating location and the inversion surface during the q_a scan. During the entire δ_a scan, the heating location was at the inversion surface.

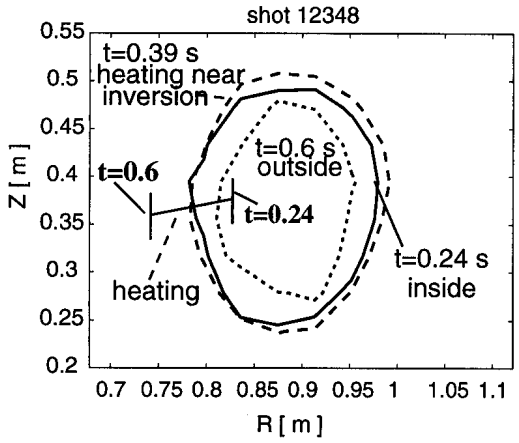

Figure 4 Change of inversion radius during a shot in which the heating location is swept by changing the magnetic field while keeping q_a constant.

The inversion surface relative to the ohmic phase is modified during ECRH and is dependent on the heating location. Heating inside the inversion surface causes it to expand, and heating outside reduces its size. Thus, the current profile is modified by different heating locations. This is shown in Figure 4 for a shot in which the heating location was changed by changing the toroidal field, keeping q_a constant by adjusting the plasma current appropriately.

After the turn-off of the heating pulse, the sawtooth *shape* returns to normal on a fast time scale, but the sawtooth *period* does not change as quickly, see figure 5; thus, there is an indication that shape and period do not depend on the same parameters.

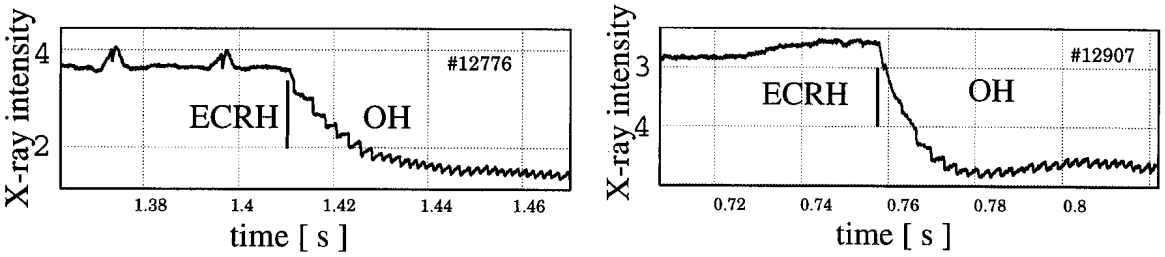

Figure 5 Sawtooth evolution near ECRH termination with partial and complete sawtooth stabilization. ECRH power 500 kW and 1 MW with heating near inversion surface.

Contrary to normal (triangular) sawteeth, the change in X-ray emissivity cannot be explained by a corresponding change in temperature for humpback sawteeth. Humpbacks always have a lower *temperature* after the crash than before the crash even though the *X-ray intensity* shows the opposite relation, as shown in Fig. 6.

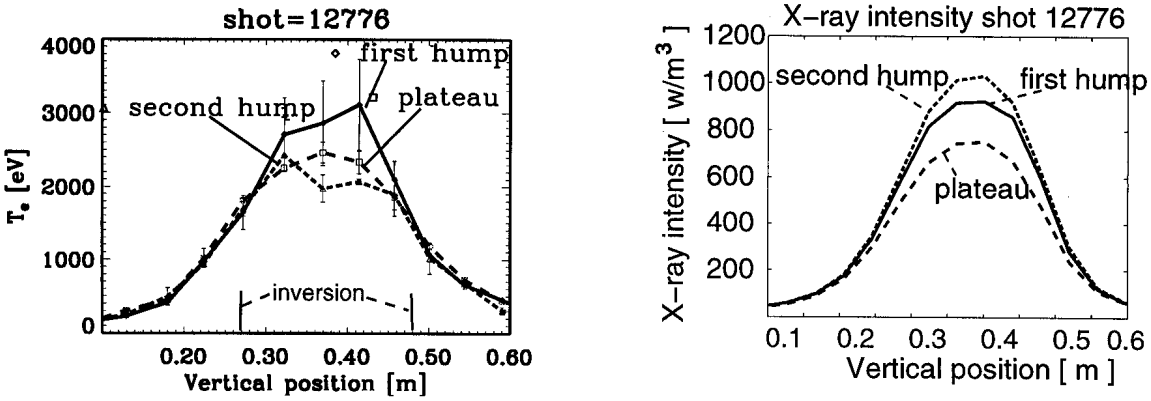

a) b)

Figure 6. Comparison of a) Thomson temperature profile and b) tomographically reconstructed local X-ray emissivity during Humpback activities taken at the same times during the shot.

Conclusions

ECRH can strongly modify sawtooth activity in the TCV plasma. In particular the sawtooth shape depends strongly on the deposition radius relative to the sawtooth inversion surface. The shape changes from triangular or humpback near the inversion surface, to saturated near the magnetic axis. The sawteeth may disappear when heating at or outside the inversion surface, leaving only Hilling activities, which can be of a very small amplitude. The effect of sawtooth shape change, is amplified by negative plasma triangularity, increasing q_a and low density. The central temperature behavior does not correspond to the central X-ray emissivity in unusual sawteeth shapes.

A previous explanation of this phenomenon, as resulting from inverse shear [Razumova, 97] in plasma produced by ECRH, is possible; however, at present TCV does not have an experimental measure of q on or near the axis. The sawteeth could be stabilized by energetic electrons generated by wave plasma interaction, but no experimental evidence of energetic electrons has been observed. Changing shear near the heating location, as suggested before [Hanada, 74] is a more plausible explanation in our case.

This work was partially supported by Swiss National Science Funds.

K. Hanada, H. Tanaka, M. Iida, S. Ide, et al Phys Rev letters. **66** (15) (1991) 1974.

K.A. Razumova, A.A. Bagdasarov, A.A. Gorshov, Yu.V. Esipchuk, D.A. Kislov, A.Ya. Kislov, N.A. Kirneva, S.E. Lysenko, A.A. Martynov, V.V. Sannikov, A.V. Sushkov, V.V. Chistyakov, Plasma Physics Reports **23**(1) (13) 1997.

Preliminary Confinement Studies during ECRH in TCV

A. Pochelon, Z.A. Pietrzyk, T.P. Goodman, M. Henderson, H. Reimerdes, M.Q. Tran, R. Behn, S. Coda, M.J. Dutch, B.P. Duval, I. Furno, F. Hofmann, J-P. Hogge, J.B. Lister, X. Llobet, Y. Martin, J-M. Moret, Ch. Nieswand, J. Rommers, O. Sauter, W. van Toledo, G. Tonetti, H. Weisen
Y.V. Esipchuk†, A.A. Martynov†

Centre de Recherches en Physique des Plasmas, Ecole Polytechnique Fédérale de Lausanne
Association EURATOM-Confédération Suisse, CH-1015 Lausanne, Switzerland

† Russian Research Centre Kurchatov, 12182 Moscow, RF

Introduction - Following extensive Ohmic heating confinement studies on various plasma shapes [Moret 97], ECRH heated experiments were started on small, low elongation plasmas in the TCV tokamak with positive and negative triangularities. For these studies, an EC power of up to 1 MW at 82.7 GHz (second harmonic X2) was injected, representing for such discharges up to 14 times the Ohmic power during EC [Pochelon 97]. When complete, the ECW system will provide 3 MW second harmonic and 1.5 MW third harmonic at pulse lengths of 2 seconds [Goodman 97]. For TCV (R = 0.89 m, a = 0.25 m, I_p < 1.2MA), the nominal field of B = 1.44 T and the frequency of 82.7 GHz place the resonance slightly on the high-field side (HFS) of the magnetic axis ($\Delta\rho$=-0.16 to -0.2). The effects of different heating localisations on confinement and MHD were studied using *1)* the mobility of the launcher mirrors (in particular for poloidal angle θ sweeps), *2)* the large vertical room for displacing the plasma in the TCV vessel and *3)* the radial displacement of the cyclotron resonance with magnetic field. Initial studies of heating and confinement have concentrated on close-to-circular plasmas to study power absorption in a large variety of beam-plasma geometries and to compare with earlier results of other machines - a necessary first step before investigating more strongly shaped plasmas.

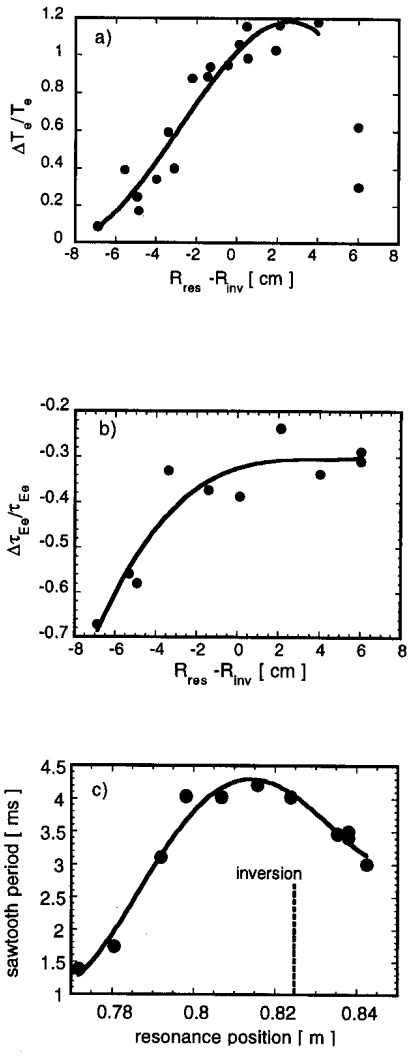

Fig. 1 Radial deposition scan relative to q=1 surface by varying B:
a) Relative T_{eo} increase, 2<q<6
b) Relative global τ_{Ee} degradation
c) Sawtooth period, q=1 position indicated
(κ=1.32, q=5, n_{eo}=2 10^{19}[m^{-3}], P_{EC}=360kW)

Confinement - To study basic confinement dependencies (B, q, n_e, P), second harmonic EC power was launched on a small target plasma placed in front of the launcher with quasi-horizontal launch in order to minimise refraction effects at high density (θ=18°, z=38, κ=1.31, δ=0.15). Scan domains were: 1.32<B<1.45T,

representing a 20% plasma radius displacement of the resonance around q=1; $1.5\times10^{19}m^{-3} < n_{eo} <$ over-dense (X2 cut-off density is $4.25\times10^{19}m^{-3}$, TORAY guaranteed full absorption up to $4.0\times10^{19}m^{-3}$); $2.2<q<6$; $P_{EC}\leq1MW$. In the q-scan, ratios of P_{tot}/P_{OH} from 3 to 14 were obtained during ECRH for 1MW power injection.

The effects of *localisation* are very important during ECRH. As an example, in a B-field scan at moderate power (0.5MW), the temperature response depends strongly on the location of power deposition relative to the inversion surface obtained from soft X-ray tomography (often assumed equal to the q=1 surface). The *central electron temperature* T_{eo} is maximum for a power deposition close to the q=1 surface (Fig. 1a); although some low q~2.5 discharges may show some increase for very central heating. The *global electron confinement time* τ_{Ee} (Fig 1b) is relatively independent of resonance position when heating inside q=1 and drops from about a/10 outside the inversion surface, meaning that efficient heating requires deposition roughly inside q=1. Data in Fig. 1 a,b) cover a large range of q values: $2.3<q<6.7$. Some low-q high-power shots may indicate a τ_{Ee} maximum (as with T_{eo}) for q~1 deposition. It is however not yet completely clear whether deposition at the magnetic axis is less efficient than heating at the q=1 surface. Nevertheless, the *sawtooth period* is maximum for q~1 deposition (Fig. 1c), which yields a dependence similar to the central electron temperature response [Pietrzyk 98].

As a function of the *safety factor q*, the confinement time τ_{Ee} increases with q, maximising at q~5 and dropping beyond (Fig. 2). In the high q shots of this scan (P_{EC}=500kW, $0.77<R_{res}<0.84$ m), the power was deposited significantly outside the q=1 surface when increasing q. The drop at high q can probably be explained by analogy to the drop observed in the radial B-field scan (Fig. 1b) when heating outside q=1. Figure 2 also contains the corresponding ohmic-confinement-time q dependence, which saturates at q>5. Even though confinement exhibits the Neo-Alcator q scaling as in ohmic plasmas [Weisen 97, Moret 97], confinement improvement with q is not as high as for ohmic heating and confinement power degradation appears stronger at high q. It is likely that higher additional power will further degrade the favourable scaling with q. In the present heating experiments, however, this beneficial ohmic scaling feature still holds for ECRH power ratios $P_{ECRH} / P_{OH} > 9$.

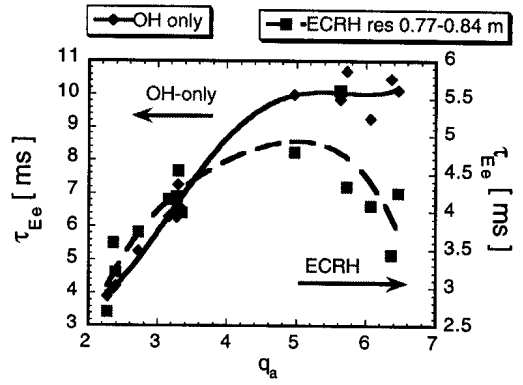

Fig. 2 τ_{Ee} versus q, for different deposition radii in a Bφ scan in ECRH, and ohmic plasmas.

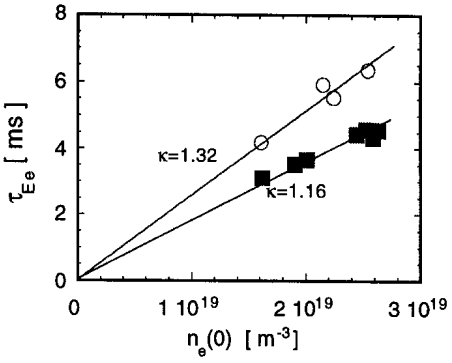

Fig. 3 τ_{Ee} as a function of n_{eo} for two elongations (κ=1.16, 1.32; δ=0.07, 0.16, q=4.7, 5.2)

The dependence of τ_{Ee} as a function of the *density* on axis is shown in Fig. 3. Low elongation plasmas (κ=1.16 and 1.32) with q≈5, located in front of the launcher to minimise refraction effects at high density, were chosen, for this scan. Heating just below

cut-off density appeared operationally difficult due to the ECRH-induced density pump-out, which explains the absence of data close to cut-off. The confinement time scales nearly linearly with density, as in previous low density EC experiments [e.g. Alikaev 85]. The two elongations covered indicate the favourable effect of elongation.

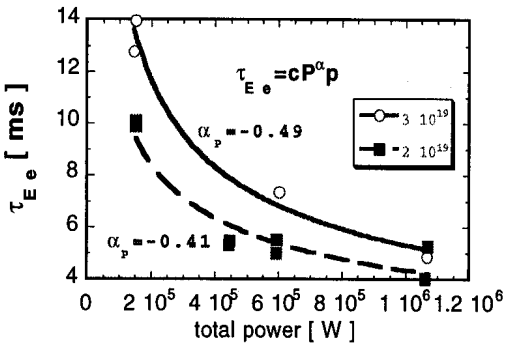

Fig. 4 τ_{Ee} power degradation for two densities, q=5

Power-induced confinement degradation was studied with 1MW of additional power. Heating results with P_{EC}>500kW contain an ECCD component since one of the launchers was placed with a non-zero toroidal angle. This should, however, have a limited effect on confinement, since power degradation in ECCD was observed to be similar to ECRH [Esipchuk 95]. The power-induced degradation exponent α_P, ($\tau_{Ee} \sim P^{\alpha_P}$), measured for q=5 at n_{eo}=2 and $3\times10^{19}m^{-3}$ (see Fig. 4), and at q=2.5 for a density close to $2\times10^{19}m^{-3}$, is as expected: $\alpha_P \sim -0.5$, or possibly somewhat lower. Note that this confinement degradation may have been influenced by the effect of slightly off-axis heating on profiles and MHD-activity. In particular, the sawtooth period is lengthened for a deposition close to q=1, and sawtooth activity is observed to disappear at the higher.

Summarising, this yields density and power exponents comparable to the ones obtained in T-10 electron cyclotron heating experiments: $\alpha_n \sim 1$, $\alpha_P \sim -0.5$ [see Alikaev 85].

The study of confinement with triangularity was done with medium q=3.5 at 500kW. The power was deposited at the q=1 surface. Both ECRH and ohmic cases are shown in Fig 5a. As with ohmic heating, confinement improves with increasing negative triangularity during ECRH. Note that the improvement of confinement with ECRH is less than with purely ohmic heating, as shown in Fig. 5b.

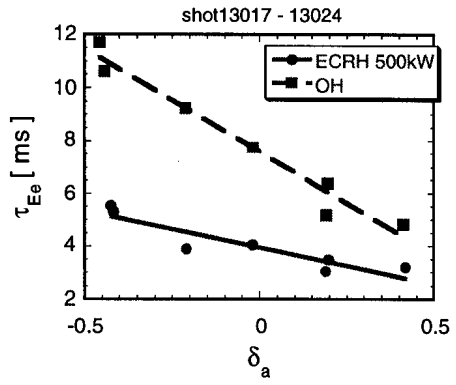

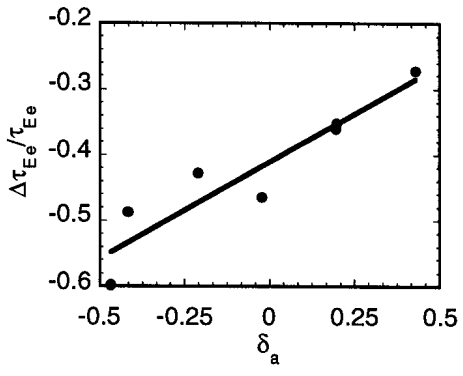

Fig. 5

a) τ_{Ee} as a function of δ, ohmic and ECRH data. (P_{EC}=500 kW, κ=1.32, q=3.5, $n_{eo}=2\ 10^{19}$ [m^{-3}]).

b) Relative τ_{Ee} power degradation as a function of δ (same data as in Fig. 5a).

Power coupling to the plasma - ECRH heated discharges have been simulated using the *ASTRA transport code*. The T-10 transport model [Dnestrovskij 93] in the ASTRA code was used without any change of transport model or coefficients and is found to reproduce the central temperature evolution of ohmic TCV discharges. In the ohmic regime, the measured TCV temperature profiles $T_e(r)$ are also well described (accuracy ±10%) by the T-10 model (i.e. similar electron transport and confinement laws can be used). To simulate correctly the measured central temperature during ECRH, it was necessary to use an absorption efficiency factor k~0.65 (where $P_{ab} = k\ P_{input}$ or more correctly, $P_{ab} = k\ P_{ab}^{TORAY}$), as in other ECRH experiments [Alikaev 85]. The T-10 model then correctly describes not only values and profiles of $T_e(r)$ and $n_e(r)$ but also the temperature responses for different power deposition profiles. Simulated discharges had sawteeth, q=3.1, κ=1.26, and oblique beam incidence angles on the resonance: $15^o<\theta<45^o$. For a non-sawtoothing discharge with high q~6, κ=1.32, $n_{eo}=2\times10^{19}m^{-3}$ in quasi-horizontal launch ($\theta=18^o$), where T_{eo}=3keV was obtained with 0.5MW, a higher k-factor, close to unity was appropriate.

The derivative of the stored energy deduced from the *diamagnetic probe* yields power coupling efficiencies similar to those from transport calculations, i.e. ranging approximately from 65 to 85%. Note that when transport calculations give good coupling, so do the diamagnetic probe measurements. The observation that the k-factor changes with the experimental configuration, while the calculated absorption from ray tracing remains constant (100%) indicates a violation of the assumptions made either in TORAY or ASTRA codes, as well as the diamagnetic loop method of determining the absorbed power.

Conclusions - Heating effects, MHD-activity and confinement depend strongly on the localisation of the EC power deposition. Sawteeth are stabilised for power deposition on q=1 and mode activity is destabilised for power deposition slightly inside the q=1 surface with corresponding effects on electron temperature: dramatic changes in central temperatures occur when heating is close to q=1 or towards the magnetic axis.

Within the range of plasma shapes and plasma currents investigated, the electron confinement time, τ_{Ee}, increases with density, elongation and negative triangularity ($0.4>\delta>-0.4$), similar to Ohmic heating. In addition, τ_{Ee} increases with q_a up to q_a~5 after which it decreases. There is little dependence of τ_{Ee} on the heating location provided it is inside the q=1 surface. As the heating location is moved outside the q=1 surface, τ_{Ee} decreases. This may be the explanation of the observed decrease in τ_{Ee} at high q_a.

The power-induced degradation exponent ($\tau_{Ee}\sim P^{\alpha_P}$) is generally as expected: $\alpha_P\sim -0.5$. However, there are some indications that the power degradation may be dependent on q_a and δ_a. In particular the power degradation may be stronger at negative triangularity.

This work was partially supported by the Fonds National Suisse pour la Recherche Scientifique.

References

V.V. Alikaev et al., Proc. 10th Int. Conf. on Plasma Phys. Cont. Nucl. Fus., **I**, 419 (1985).
Y.N. Dnestrovskij, D.P. Kostomarov, WO "Nauka", Moscow, 1993/ Springer Verlag 1986
Y. Esipchuk et al., J. Moscow Phys. Soc. **1**, 119 (1991) and ITER-IL-PH-4-9-5-10 (1991).
Y. Esipchuk, Plasma Phys. and Contr. Fus. **37**, Suppl. 11A, A267 (1995).
T.P Goodman et al., Proc. EC-10 Conf., presented by M.Q. Tran, Ameland 1997.
J.-M. Moret et al., Phys. Rev. Lett. **79**, 2057 (1997).
Z.A. Pietrzyk et al., this Conf.
A. Pochelon et al., 24th EPS Conf. on contr. Fus. and Plasma Phys., **21A**, PartII, 537(1997).
H. Weisen et al., Nucl. Fus. **37**, 1741 (1997).